RAA 2019 Vol. **19** No. **9**, 130(18pp) doi: 10.1088/1674–4527/19/9/130

http://www.raa-journal.org *http://iopscience.iop.org/raa*

Research in Astronomy and Astrophysics

Orbital evolution of a planet with tidal dissipation in a restricted three-body system

Wen-Lei Wang[1,2,3], Xue-Qing Xu[1,2] and Xin-Hao Liao[1,2]

[1] Shanghai Astronomical Observatory, Chinese Academy of Sciences, Shanghai 200030, China; *wangwl@shao.ac.cn, xhliao@shao.ac.cn*

[2] Key Laboratory of Planetary Sciences, Shanghai Astronomical Observatory, Chinese Academy of Sciences, Shanghai 200030, China

[3] University of Chinese Academy of Sciences, Beijing 100049, China

Received 2019 March 24; accepted 2019 April 16

Abstract The angle between planetary spin and the normal direction of an orbital plane is supposed to reveal a range of information about the associated planetary formation and evolution. Since the orbit's eccentricity and inclination oscillate periodically in a hierarchical triple body and tidal friction makes the spin parallel to the normal orientation of the orbital plane with a short timescale in an isolated binary system, we focus on the comprehensive effect of third body perturbation and tidal mechanism on the angle. Firstly, we extend the Hut tidal model (1981) to the general spatial case, adopting the equilibrium tide and weak friction hypothesis with constant delay time, which is suitable for arbitrary eccentricity and any angle ϑ between the planetary spin and normal orientation of the orbital plane. Furthermore, under the constraint of angular momentum conservation, the equations of orbital and ratational motion are given. Secondly, considering the coupled effects of tidal dissipation and third body perturbation, and adopting the quadrupole approximation as the third body perturbation effect, a comprehensive model is established by this work. Finally, we find that the ultimate evolution depends on the timescales of the third body and tidal friction. When the timescale of the third body is much shorter than that of tidal friction, the angle ϑ will oscillate for a long time, even over the whole evolution; when the timescale of the third body is observably larger than that of the tidal friction, the system may enter stable states, with the angle ϑ decaying to zero ultimately, and some cases may have a stable inclination beyond the critical value of Lidov-Kozai resonance. In addition, these dynamical evolutions depend on the initial values of the orbital elements and may aid in understanding the characteristics of the orbits of exoplanets.

Key words: astrometry and celestial mechanics: celestial mechanics — planet-star interactions — planets and satellites: dynamical evolution and stability

1 INTRODUCTION

In recent years, the discovery of a large population of exoplanets has greatly enriched our current theories of planetary formation and evolution. The statistical characteristics of exoplanets also suggest that exoplanets can be very different from planets in our solar system, with eccentricities ranging from nearly zero to one (Hugh et al. 2006; Barge et al. 2008; Keivan et al. 2018). Although the McLaughlin effect is taken into account, not all of the inclination angles are small, and there are both prograde and retrograde orbits with large inclination angles of these exoplanets (Welsh et al. 2012; Kostov et al. 2016). Meanwhile, their semi-major axes (SMAs) also vary from a few astronomical units, which are very close to the central object, to hundreds of astronomical units (Kalas et al. 2008; Beust et al. 2014). In particular, there are gas giant planets close to the host star, some of which have anomalous radii (Mayor & Queloz 1995; Marcy et al. 2005). The above statistical features also demonstrate the fact that planets close to their host stars would be affected by stellar tidal dissipation (Mardling 2007; Wu 2018).

Tides are a widespread natural phenomenon in the universe, as is well known, from the Earth-Moon system (Peale & Cassen 1978) to other planets and their moons in the solar system (Yoder & Peale 1981; Showman & Malhotra 1997; Peale & Lee 2002), exoplanets and their host stars (Rasio et al. 1996; Jackson et al. 2008b), binary

star systems and galaxies (Zahn 1977; Mazeh 2008). Tidal dissipation can not only change the configuration of the system, but also alter the geological structure of celestial bodies. In detail firstly, tides reduce the energy of a system, causing the orbits of celestial bodies to decay into an equilibrium or collision occurs (Jackson et al. 2008a; Dong & Ji 2012; Husnoo et al. 2012; Lai 2012; Guillot et al. 2014) and also affect the rotational evolution (e.g., Bodenheimer et al. 2001; Pont 2009; Lanza 2010; Ibgui et al. 2011; Poppenhaeger & Wolk 2014; Ceillier et al. 2016). Secondly, the heat caused by tidal friction keeps heating the celestial body constantly, causing radial expansion or volcanic eruptions. For instance, in the Earth-Moon system, under the influence of terrestrial tides, the Moon has entered into the co-rotation state, and its orbital eccentricity has also been circularized (Auclair-Desrotour et al. 2018b). Under the influence of tidal dissipation, volcanic eruptions occur on Jupiter's moon Io (Yoder & Peale 1981; Aksnes & Franklin 2001), where tides are raised on one by the other, due to the effect of the gravitational gradient or variation of gravitational force across the body.

Research shows that the intensity of tidal dissipation is mainly determined by the distance and internal quality factor of celestial bodies: the closer the distance, the stronger the tidal dissipation and vice versa. The internal quality factor is related to the internal structure of a planet (Goldreich & Soter 1966; Socrates et al. 2012), and the quality factors of different layers are different in a hierarchical model (Storch & Lai 2014; André et al. 2017). Meanwhile, since a celestial body is not completely elastic and is viscous, the response of tidal deformation will be delayed. In addition, rotation and revolution will cause tidal bulge deviation along the line between the celestial body centers. In general, the dynamic tide and equilibrium tide are the main mechanisms in the tidal model. Currently, the analytical theories of tidal action in extrasolar planets are mostly based on equilibrium tide and weak friction approximations, which originate from the classical tidal theory of Darwin (1879, 1880), and Darwin's theory was extended in the process of studying close binaries and exoplanets (Goldreich 1963; Kaula 1964; Alexander 1973; Zahn 1977; Hut 1981; Eggleton et al. 1998). The equilibrium tide assumes that the deformation of celestial bodies could happen instantaneously under tidal force. As an improvement to the equilibrium tide model, the weak friction approximation postulates that there is some delay in the tidal bulge, mainly because of the non-ideal elasticity of natural bodies. In the processes of dissipative parameterization, the most common prescriptions are either a constant phase lag (constant-Q) model (Goldreich & Soter 1966) or a constant time lag (constant-τ) model (Wisdom 2008; Leconte et al. 2010b). Although the sources of variability in the two tidal models are fundamentally different, they are often mistakenly mixed together (Ferraz-Mello et al. 2008). Indeed, in the constant-τ model, the phase delay is linearly dependent on the time delay. Calculations could be carried out in terms of a closed formula for any eccentricity with the constant-τ model (Leconte et al. 2010a). High order computation based on eccentricity is very cumbersome and troublesome in the framework of the constant-Q model. Leconte et al. (2010b) pointed out that if the perturbation function in the constant-Q model was expanded to a lower eccentricity order, it would inevitably produce incorrect results when the eccentricity exceeded 0.2. Taking the above into account, the constant-τ model is selected in our research, with the case of high eccentricity and high inclination angle.

Hut (1980, 1981) systematically studied tidal dissipation in close binary star systems. In his model, variations of the SMA, orbital eccentricity and rotation rate were considered, but only when the normal direction of the orbital plane was nearly parallel to the rotation direction, and he also neglected the effects of longitude of the ascending node, pericenter and rotation direction (Hut 1981). The results showed that when the system angular momentum was not less than the critical angular momentum corresponding to the minimum energy of the system, the system would evolve into an equilibrium state. When no less than three-quarters of the system angular momentum existed in the form of orbital angular momentum, the equilibrium state was stable (Hut 1980). In this paper, a spatial tidal dissipation model is established based on the Hut model, and the motion equation of tidal dissipation is given. This model also adopts the hypothesis of weak friction, and can be applied to arbitrary eccentricity and angle ϑ, where ϑ refers to the spatial angle between the direction of rotation and the normal direction of the orbital plane. When ϑ is zero, it will degenerate into a trivial situation. Meanwhile, this model is suitable for the evolution of tidal dissipation under high eccentricity, but also reveals the state of system evolution before and after ϑ approaches zero. It is notable that this paper considers the planets' deformation due to the tidal effects of stars in the spatial tidal dissipation model, which is different from the case of considering the tidal effect of planets on stars and the rotation of stars adopted in other tidal dissipation models (Naoz et al. 2012; Anderson et al. 2016; Xue et al. 2014). In order to simplify the problem, we only consider the rotation of planets and ignore the rotation of stars.

The tidal force is very large when a planet moves to the pericenter of a large elliptical orbit, which could cause intense tidal dissipation, significant orbital migration of the planet, and makes the planet evolve to a position close to the star (Heller et al. 2011; Anderson et al. 2016). The major factor in producing a large ellipse is the third body perturbation and, therefore, this paper simultaneously con-

siders the effects of external-type three-body perturbation and tidal dissipation, to establish a comprehensive model (CPM). Specifically, the quadrupole moment approximation of the third body perturbation is adopted in this model (Clifford 2017; Wang et al. 2018). When the orbital eccentricity is large, the tidal effect is relatively large near the pericenter in the CPM, which would cause the system energy to reduce and the orbit to become gradually smaller and rounder. Since the orbit's eccentricity and inclination oscillate periodically in a hierarchical triple body and tidal friction makes the spin parallel to the normal orientation of the orbital plane with a short timescale in an isolated binary system, the evolution of the angle ϑ may be more complicated and interesting in the CPM. In detail, the timescale of the third body exciting the inclination and the timescale of the tide affecting the spin parallel to the orbital normal direction will decide the evolution path of the dynamic system differently from the single mechanism. Based on the above conjecture, this paper tries to reveal some unique mechanisms for the evolution of orbit and rotation under the coupled effect of tidal dissipation and third body perturbation.

In Section 2, a spatial tidal dissipation model is established according to the time-delay model. In order to study the long-term effect, the tidal perturbation function is averaged over the orbital period. Then based on the constraint of angular momentum conservation, the corresponding motion equations of the planet rotation direction and rotation rate can be obtained. Finally, the quadrupole moment approximation effect of the third body perturbation is added on the basis of the tidal dissipation model, and the CPM considering the third body perturbation and the tidal dissipation is obtained. In Section 3, since the third body excites eccentricity and inclination oscillation periodically, the angle between the rotation orientation and the normal direction of the orbital plane will oscillate for a long time during the evolution process. In Section 4, we focus on those systems which eventually tend to stable states, and find that the tidal dissipation has an inhibiting effect on the long-term perturbation of the third body, and in these states the periodic oscillations of orbital inclination angle no longer occur in the system, even if the orbital inclination is in the Lidov-Kozai (LK) resonance region. In Section 5, the main conclusions are given, and the rationality of the hypothesis and future work are discussed.

2 THE MODELS

In a star-planet system, the energy of the planet's orbit as well as exchanges between orbital and rotational angular momentum would be changed by stellar tidal dissipation. The famous tidal models can be divided into two types: equilibrium tide and dynamic tide. For dynamic tides, viscoelastic coefficients and the thickness of different layers

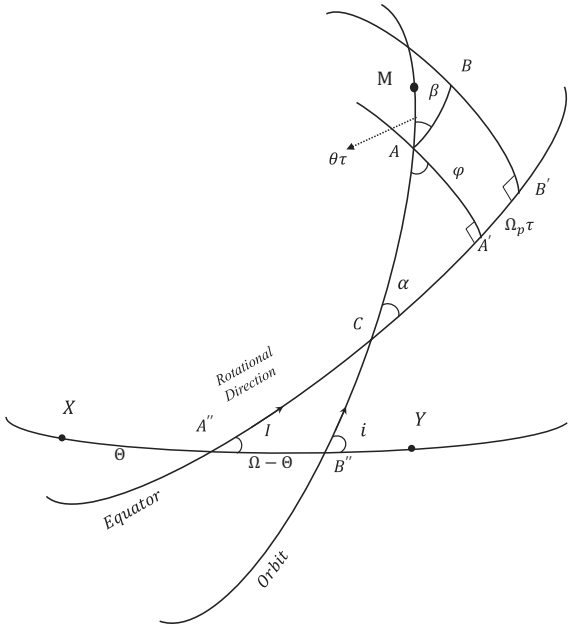

Fig. 1 The tidal deformation of a binary system in the $Oxyz$ coordinate system.

in the interior of the planet should be considered, such as stratification theory (Storch et al. 2014). If the planet is within its Roche limit, mass may be stripped from it to the star under tidal dissipation (Faber et al. 2005). Tidal heating will also change the radius and radiation from the star will cause a thermal tide, which may result in a larger radius and coupling with the gravitational tide (Gold & Soter 1969; Arras & Socrates 2010; Auclair-Desrotour et al. 2015, 2017, 2018a). If the planet is Earth-like, multiple layers in its internal structure will enhance the dissipation and influence the climate and habitability (Tobie et al. 2005; Henning & Hurford 2014; Breton et al. 2018; Turbet et al. 2018). For the equilibrium tide model, the planets are assumed to be perfectly elastic rigid bodies. Tidal deformation will arise and form an instantaneous equipotential shape, when a planet is in the gravitational field of a star. The planetary radius will be stretched along the line joining the two mass centers. Furthermore, the weak friction model assumes that the planet is a rigid body with viscoelasticity, and the tidal bulge of the planet will be somewhat delayed under the tidal forces (Alexander 1973). The delay determined by the planetary internal quality factor can be described by phase delay or time delay. Leconte et al. (2010b) discussed the difference between phase delay and time delay, and pointed out that the phase delay model would be wrong when used for large elliptical orbits. The time delay of gas planets is usually obtained by the relative relationship between Jupiter and one of its moons, and the magnitude is about 0.062–0.66 s (Goldreich & Soter 1966; Socrates et al. 2012). Since the planet's rotation rate

is inconsistent with its revolution rate, the tidal bulge will further deviate from the two centroid lines.

Kozai (1965) established the general tidal model based on the equilibrium tidal model and the weak friction approximation, to study the influence of terrestrial tidal deformation on satellites of the Earth. This model assumes that tidal deformations on Earth are mainly caused by the Sun and Moon, not by satellites. The Hut tidal model (Hut 1981) was mainly used to examine the evolution of close binaries under tidal effects. Hut firstly considered the case where angle $\vartheta = 0$, and then extended to the linear order case. Wisdom (2004, 2008) presented a general model, which contained a planet and its synchronously rotating satellite, mainly taking into account the existence of arbitrary angle and eccentricity. To understand the coupling effects between tides and the third body perturbation, this work extends the Hut tidal model (Hut 1981) to a general spatial tidal model, which would be applicable to arbitrary eccentricity and angle ϑ. We obtain the equation of planetary rotation with conservation of total angular momentum, and the models are described below.

2.1 General Spatial Tide Model

To simplify the problem, we only consider the tidal deformation of a planet by a star, and ignore the tidal effect of the planet on the star. In addition, we will not be concerned about whether the angle ϑ is zero or not, or whether the eccentricity of the planet is small or large. Because natural planets are not perfectly elastic but rather viscoelastic, the tidal deformation is not instantaneous and there will be a lag angle ψ between the tidal bulge and the line joining the centers of the star and planet, which can be expressed by the time delay τ. Assuming that r is the distance between the planetary center and the center of the star at time t, the planetary deformation is caused by the star at time $(t-\tau)$, which corresponds to r' as the distance between the centers of the two bodies.

While the spin of the planet is parallel to the orbital angular momentum, namely $\vartheta = 0$, if the planetary rotation speed Ω_p is greater than the instantaneous orbital angular velocity $\dot{\theta}$, then the tidal bulge is in front of the line joining the centroid of the planet and star, and vice versa, and the included angle $\psi = (\Omega_p - \dot{\theta})\tau$. Since the angle $\vartheta = 0$, the tidal perturbation forces only have two components in the orbital plane radial direction $\hat{r}$ and the transverse direction $\hat{\theta}$, and the part is zero in the orbital plane normal direction $\hat{w}$, in which $\hat{r}$, $\hat{\theta}$ and $\hat{w}$ are the unit vectors of the three directions respectively. Following the Hut model (Hut 1981), only the leading order (quadrupole) of the angle ψ and the terms linear in τ will be treated, and then the tidal perturbation forces can be represented by

$$\boldsymbol{F_{tr}} = -3k_2\frac{GM^2}{r^2}\Big(\frac{R}{r}\Big)^5(1+3\frac{\dot{r}}{r}\tau)\hat{r}\,, \tag{1}$$

$$\boldsymbol{F_{t\theta}} = 3k_2\frac{GM^2}{r^2}\Big(\frac{R}{r}\Big)^5(\Omega_p-\dot{\theta})\tau\hat{\theta}\,. \tag{2}$$

Here, G is the universal gravitation constant and R is the radius of the spherical planet. M and m are the stellar mass and planetary mass respectively, and k_2 is the main-order Love number. Different types of planets have different Love numbers, which are related to the composition of the planet, such as being a solid or gas planet, and the internal structures of the planet. For a gas giant planet, k_2 is between $0.1-0.01$ (Xue et al. 2014).

When the tidal model is extended to the general spatial case, the rotation and revolution of the planets are out of sync, and the orbital plane of the planet does not coincide with the equatorial plane of the star. Considering the above two points, a central coordinate system is chosen with the central star as the origin O, and the OXY plane coinciding with the equatorial plane of the star. As the planet spins and revolves at the same time, the effect of revolution is firstly considered. The tidal bulge will lag $\dot{\theta}\tau$ behind the line joining the centers of the star and planet with the effect of revolution, and the position is A (see Fig. 1). Then the effect of rotation is taken into account and, for simplicity, assuming that the rotation and revolution are in the same direction, the tidal bulge will move from A to B.

$\hat{AB}$ is an arc on a small circle, which can be approximated as an arc on a great circle, then $\hat{AB}$ is approximately equal to $\Omega_p\tau\cos\varphi$. It is notable that STW is the coordinate system based on radial, transverse and orbital plane normal unit vectors $\hat{r}$, $\hat{\theta}$ and $\hat{w}$ respectively. So, arc $\hat{AB}$ in STW can be expressed by orbital elements. The projection of $\hat{AB}$ in the orbital plane radial direction $\hat{r}$ is 0, which means that the radial component force of the general spatial model stays the same as in Equation (1), and the projection of $\hat{AB}$ in the orbital plane transverse direction $\hat{\theta}$ is

$$\Omega_p\tau\cos\varphi\cos\beta \triangleq \Omega_p\tau A\,. \tag{3}$$

The projection of $\hat{AB}$ in the orbital plane normal direction $\hat{w}$ is

$$\Omega_p \tau \cos\varphi \sin\beta \triangleq \Omega_p \tau(\cos(u)B + \sin(u)C)\,, \tag{4}$$

in which, A, B, C and D are

$$\begin{cases} A = \cos I \cos i + \sin I \sin i \cos(\Omega - \Theta), \\ B = \cos I \sin i - \sin I \cos i \cos(\Omega - \Theta), \\ C = \sin I \sin(\Omega - \Theta), \\ D = \sin i \sin(\Omega - \Theta). \end{cases} \tag{5}$$

Here, $u = f + \omega$, f is the true anomaly, ω is the argument of pericenter, Ω is the orbital longitude of the ascending node and i is the orbital inclination. I represents the inclination of the equatorial plane of the planet and Θ is the longitude of the ascending node of the planet's equatorial plane if the direction of rotation is positive. Considering the force between two point masses, the perturbing force between two celestial bodies is decomposed into

$$\boldsymbol{F} = -\frac{GMm}{r^2}\Big\{\hat{r} + 3\frac{M}{m}\Big(\frac{R}{r}\Big)^5 k_2[(1 + 3\frac{\dot{r}}{r}\tau)\hat{r} - (\Omega_p - \dot{\theta})\tau)\hat{\theta} + \Omega_p\tau(B\cos(u) + C\sin(u))\hat{w}]\Big\}\,. \tag{6}$$

The first term is the universal gravitation between the two point masses, while the others represent a tidal perturbing force. The corresponding acceleration can be expressed as

$$\ddot{\boldsymbol{r}} = -\frac{GMm}{r^2}\hat{r} + S\hat{r} + T\hat{\theta} + W\hat{w} \tag{7}$$

where S, T and W are the components of perturbed acceleration in three directions, which are respectively

$$\begin{cases} S = -3\frac{\mu}{r^2}\frac{M}{m}\Big(\frac{R}{r}\Big)^5 k_2(1 + 3\frac{\dot{r}}{r}\tau), \\ T = 3\frac{\mu}{r^2}\frac{M}{m}\Big(\frac{R}{r}\Big)^5 k_2(\Omega_p - \dot{\theta})\tau), \\ W = -3\frac{\mu}{r^2}\frac{M}{m}\Big(\frac{R}{r}\Big)^5 k_2\Omega_p\tau[B\cos(u) + C\sin(u)]. \end{cases} \tag{8}$$

Here $\mu = G(M+m) = n^2a^3$, n is the mean orbital angular velocity and a is the orbital SMA. When the rotation direction is parallel to the normal direction of the orbital plane, namely $\vartheta = 0$, then $\Omega = \varphi$, $i = I$, $A = 1$, $B = 0$, $C = 0$ and then Equation (8) is consistent with equation (8) in Hut (1981). For any isolated binary system, the tidal effect makes the total mechanical energy dissipate gradually, while the total angular momentum is conserved. Three quantities are required to describe the rotational angular momentum in space: the magnitude of rotational velocity Ω_p and two direction angles I and Θ. The motion equations can be obtained from conservation of angular momentum. The planet's orbital angular momentum is $J = Mm/(M+m)\sqrt{\mu p}$, where $p = a(1-e^2)$ is the semilatus rectum. The angular momentum of the system is $J\hat{w} + I_p\Omega_p\hat{N} = \boldsymbol{C}$, $\boldsymbol{C}$ is a constant vector and the square of the radius of gyration r_g^2 is defined as $I_p = mR_p^2r_g^2$, where I_p is the moment of inertia of the primary (for a homogeneous gas giant, $r_g^2 = 0.4$, and for a real gas giant, r_g^2 is between about 0.01 and 0.1) (Hut 1981). $\hat{N}$ is the unit vector for the planetary rotation speed. By taking the derivative of both sides of the conservation equation with respect to time, the equation of spin angular momentum motion can be given by

$$\frac{dI_p\Omega_p\hat{N}}{dt} = -rF_\theta\hat{\omega} + rF_w\hat{\theta} \tag{9}$$

where F_θ and F_w are the components of $\boldsymbol{F}$ in $\hat{\theta}$ and $\hat{w}$, respectively. There is a three dimensional vector in the right-hand side of Equation (9), which depends on the orbital elements and can be represented by $(N_x, N_y, N_z)^T$. Through simplification and naturalization, the resulting equations of rotational motion are

$$\begin{cases} \frac{d\Omega_p}{dt} = \frac{(N_x\sin\Theta - N_y\cos\Theta)\sin I + N_z\cos I}{I_p}, \\ \frac{dI}{dt} = \frac{(N_x\sin\Theta - N_y\cos\Theta)\cos I + N_z\sin I}{I_p\Omega_p}, \\ \frac{d\Theta}{dt} = \frac{N_x\cos\Theta + N_y\sin\Theta}{I_p\Omega_p}. \end{cases} \tag{10}$$

Based on the tidal equilibrium model and weak friction approximation, this part establishes the equation of motion for the general tidal model in space, which is suitable for arbitrary eccentricity, arbitrary orbital inclination and arbitrary included angle Θ. In order to improve operation efficiency and save calculation time, if the eccentricity is less than 10^{-5}, then the eccentricity will be considered to be zero in the process of numerical calculation; and to study the long-term effects of tidal dissipation, the equations of motion are usually averaged.

2.2 Averaged Tide Model

To investigate secular effects of the tide, short-period terms should be eliminated by averaging the orbit over the orbital period P. Generally, the averaging method is $\bar{F} = \frac{1}{P}\int_0^P F(t)dt$. Here, the function does not only directly contain time t, but also contains quantities that vary with time, such as r, $\dot{r}$, $\dot{\theta}$, f and E. By using the basic formulas of celestial mechanics, those quantities can be transformed into a suitable anomaly which contains true anomaly f or eccentric anomaly E. Specifically, by averaging the equations of orbital motion and rotation under the tidal perturbation in Section 2.1, we can obtain the equations of orbital motion as

$$\begin{cases} \frac{da}{dt} = -6\frac{k_2}{T_t}\frac{M}{m}q(\frac{R}{a})^8 a(1-e^2)^{-\frac{15}{2}}[f_1(e^2) - f_2(e^2)(1-e^2)^{\frac{3}{2}}\frac{\Omega_p A}{n}] , \\ \frac{de}{dt} = -27\frac{k_2}{T_t}\frac{M}{m}q(\frac{R}{a})^8 e(1-e^2)^{-\frac{13}{2}}[f_3(e^2) - \frac{11}{18}f_4(e^2)(1-e^2)^{\frac{3}{2}}\frac{\Omega_p A}{n}] , \\ \frac{di}{dt} = -\frac{3}{2}\frac{k_2}{T_t}\frac{M}{m}q(\frac{R}{a})^8\frac{\Omega_p}{n}(1-e^2)^{-5}[\frac{3}{2}e^2 f_6(e^2)(B\cos 2\omega + C\sin 2\omega) + Bf_5(e^2)] , \\ \frac{d\Omega}{dt} = -\frac{3}{2}\frac{k_2}{T_t}\frac{M}{m}q(\frac{R}{a})^8\frac{\Omega_p}{n\sin i}(1-e^2)^{-5}[\frac{3}{2}e^2 f_6(e^2)(B\sin 2\omega - C\cos 2\omega) + Cf_5(e^2)] , \\ \frac{d\omega}{dt} = \frac{15}{2}k_2\frac{M}{m}(\frac{R}{a})^5 n f_4(e^2)(1-e^2)^{-5} - \cos i\frac{d\Omega}{dt} . \end{cases} \tag{11}$$

Correspondingly, the equations of rotational variation have the following concrete forms

$$\begin{aligned} \frac{d\Omega_p}{dt} = K_T\Omega_p(1-e^2)^{-\frac{9}{2}} \Big[& 2\big(\tfrac{n}{\Omega_p}A(1-e^2)^{-\frac{3}{2}}f_2(e^2) - A^2 f_5(e^2)\big) \\ & - f_4(e^2)(B\sin\omega - C\cos\omega)^2 - f_7(e^2)(B\cos\omega + C\sin\omega)^2\Big] , \end{aligned} \tag{12}$$

$$\begin{aligned} \frac{dI}{dt} = K_T(1-e^2)^{-\frac{9}{2}} \Big[& 2\Big(AB' f_5(e^2) - \tfrac{n}{\Omega_p}B'(1-e^2)^{-\frac{3}{2}}f_2(e^2)\Big) \\ & + f_4(e^2)(B\sin\omega - C\cos\omega)(A'\sin\omega + C'\cos\omega) \\ & + f_7(e^2)(B\cos\omega + C\sin\omega)(A'\cos\omega - C'\sin\omega)\Big] , \end{aligned} \tag{13}$$

$$\begin{aligned} \frac{d\Theta}{dt} = \frac{K_T}{\sin I}(1-e^2)^{-\frac{9}{2}} \Big[& 2\Big(\tfrac{n}{\Omega_p}D(1-e^2)^{-\frac{3}{2}}f_2(e^2) - AD f_5(e^2)\Big) \\ & + f_4(e^2)(B\sin\omega - C\cos\omega)(D'\sin\omega - \cos\omega\cos(\Omega-\Theta)) \\ & + f_7(e^2)(B\cos\omega + C\sin\omega)(D'\cos\omega + \sin\omega\cos(\Omega-\Theta))\Big] , \end{aligned} \tag{14}$$

where

$$\begin{aligned} & f_1(e^2) = (1 + \frac{31}{2}e^2 + \frac{255}{8}e^4 + \frac{185}{16}e^6 + \frac{25}{64}e^8) , \quad f_2(e^2) = (1 + \frac{15}{2}e^2 + \frac{45}{8}e^4 + \frac{5}{16}e^6) , \\ & f_3(e^2) = (1 + \frac{5}{4}e^2 + \frac{15}{8}e^4 + \frac{5}{64}e^6) , \qquad f_4(e^2) = (1 + \frac{3}{2}e^2 + \frac{1}{8}e^4) , \\ & f_5(e^2) = (1 + 3e^2 + \frac{3}{8}e^4) , \qquad f_6(e^2) = (1 + \frac{1}{6}e^2) , \\ & f_7(e^2) = (1 + \frac{9}{2}e^2 + \frac{5}{8}e^4) , \end{aligned}$$

and,

$$T_t = \frac{R^3}{Gm\tau} , \tag{15}$$

is a typical timescale of tidal dissipation. It is inversely proportional to the tide delay factor τ. In the constant time delay model, T_t is constant. The timescale factor of rotation can be regarded as K_T

$$K_T = \frac{1}{I_p}[\frac{3}{2}\frac{k_2}{T_t}\frac{M^2}{m}\frac{R^8}{a^6}] . \tag{16}$$

$q = (\frac{M}{m} + 1)$ signifies the mass ratio between stars and planets. Furthermore A', B', C' and D' are

$$\begin{cases} A' = \sin I\sin i + \cos I\cos i\cos(\Omega - \Theta), \\ B' = \sin I\cos i - \cos I\sin i\cos(\Omega - \Theta), \\ C' = \cos I\sin(\Omega - \Theta), \\ D' = \cos i\sin(\Omega - \Theta). \end{cases} \tag{17}$$

In the process of evolution, if the system eventually enters the state where the normal direction of the orbital plane is parallel to the direction of rotation, namely $i = I$ and $\Omega = \Theta$, then Equations (8) and (17) can be abbreviated as $A = 1$,

$B = C = D = 0$, $A' = 1$ and $B' = C' = D' = 0$, and then $di/dt = dI/dt = 0$ and $d\Omega/dt = d\Theta/dt = 0$. In this case, the orbital motion equations given in Equation (11) are reduced to Hut's equations (9) and (10). Meanwhile, the rotation equations, Equations (12)−(14), will be reduced to Hut's equation (11), and therefore, that is to say, the model in this paper covers Hut's tidal model. In addition, if the system will eventually reach a round state, namely the eccentricity $e = 0$, $\frac{d\omega}{dt}$ will degenerate into $\frac{d\omega}{dt} = \frac{15}{2} k_2 \frac{M}{m} (\frac{R}{a})^5 n$. So, ω only increases linearly with time when the system enters a stable state. That is why Hut neglected the motion of ω for isolated binary systems.

2.3 Model Comparison

For convenience of calculation, mass and distance are normalized with the mass of the Sun $M_\odot$ as the basic unit of mass and the average distance between the Sun and the Earth (1 AU) as the basic unit of length. Also to make the gravitational constant $G = 1$, the corresponding time unit is $T_{\rm normal} = \sqrt{\rm AU^3/GM_\odot}$. In this paper, the mass of the central celestial body is assumed to be equal to the mass of the Sun, $M = M_\odot$, and the planet is considered to be a Jupiter-like gas planet, $m = 10^{-3}\, M_\odot$, whose planetary radius is $R = 8.0 \times 10^{-4}$ AU, the 2nd-order Love number is $k_2 = 10^{-1}$, the square of radius of gyration $r_g^2 = 0.01$ and the tidal lag time τ is 0.6 s (Xue et al. 2014). In addition, the Runge-Kutta 7th(8th) order integrator is adopted in the numerical calculation.

In order to verify the validity of the averaged model, Figure 2 compares the averaged model and the numerical model under the general spatial tidal model. Specifically, the orbital initial parameters are $a = 10^{-1}$ AU, $e = 0.8$, $i = 70°$, $\Omega = 40°$, $\omega = 5°$ and $M = 0$. The initial rotation period is $T_p = 10$ h, and $I = 60°$, $\Theta = 30°$, where the relation between rotation period and rotation speed is $T_p = 2\pi/\Omega_p$. Note that the ordinate Ω_p/n takes the logarithm of $\log_{10}$, in the same way as in the following figures. Also, the mean orbital angular velocity n refers to the instantaneous angular velocity of revolution for the numerical model. Results in Figure 2 show that the SMA a eventually decays to a certain degree, and then to a stable state. Meanwhile, the eccentricity would also decay to zero (circular) slowly. In addition, the rotation and revolution would enter into a 1:1 resonance (co-rotation) case. In the general model, the equatorial tilt angle I and orbital inclination i tend to converge very quickly (co-planar, $\vartheta = 0$) within a short time. Furthermore, since the timescale of ϑ decay is so short, whether the orbital inclination and rotation direction are consistent or not would weakly affect the overall relative evolution of an isolated binary system. Generally, since the general numerical model contains the short-period term, the ratio of the rotational rate and instantaneous orbital angular velocity has short-period oscillations during the evolution process, which means that Ω_p and n are oscillating towards resonance. The initial orbital parameters in Figure 2 are the high eccentricity and high inclination. This is a typical example for the general tidal dissipation model, and indicates that the general tidal model is suitable for the case of high eccentricity and high orbital inclination.

2.4 The Third-body Perturbation

The third-body perturbation has useful applications for different systems from planetary to stellar scales. In Jacobi coordinates, the perturbed functions have been expanded up to the hexadecapole order with the SMA ratio, which has a unified form of internal and external perturbation (Wang et al. 2018). Further, preliminary studies were made under restrictive conditions. Results show that the influence of hexadecimal moment approximation cannot be neglected in some configurations. The third-body model would be added to other comprehensive effects (e.g., tidal effects, post-Newtonian effects, etc.). When considering the coupling effect of the spatial tidal dissipation and third-body perturbation, in particular, the planet is not only deformed by the stellar tide, but also affected by the perturbation of the third body m', which is called the CPM. In this paper, to clarify problems, some new basic assumptions in the CPM are adopted. The mass of the perturbed body m is much smaller than that of the central body M and third body m'. Additionally, only the rotation of the body m is considered, and the rotation of the central body and third body are ignored in the CPM. Those assumptions simplify the CPM as much as possible, and these factors can also be taken into account in subsequent studies.

In the numerical calculations, we adopt the orbital surface of the perturbing body as the reference plane and assume that it orbits circularly, namely $i' = 0°$ and $e' = 0$. Since only the quadrupole approximation is considered, the longitude of the ascending node and the argument of the perturbing body pericenter are ordinary. The third body perturbation function can be obtained in the central coordinate system to be suitable for the tidal model.

$$U_{\rm tb} = -\frac{Gm'}{16}\frac{a^3}{a'^3}\Big[(3\sin^2 i - 2)(2+3e^2) - 15e^2\sin^2 i\cos 2\omega\Big], \tag{18}$$

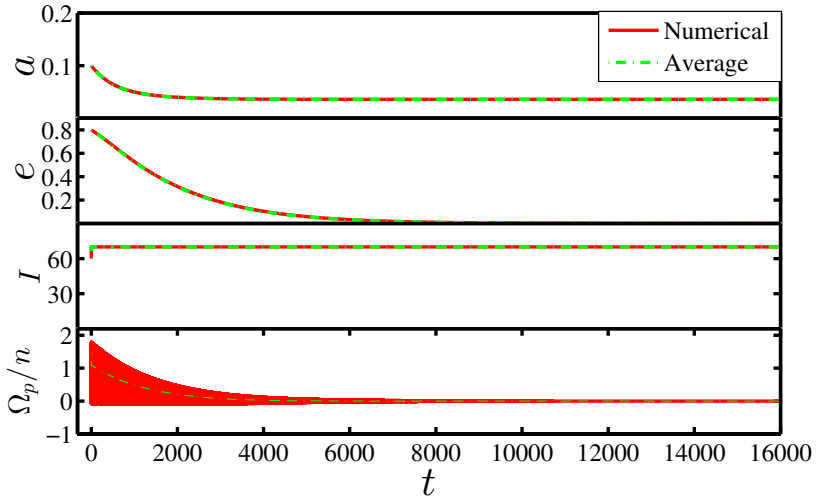

Fig. 2 Comparisons between the numerical tidal model and average tidal model.

where a' is the SMA of the perturbing body. The resulting third-body perturbation equations are

$$\begin{cases} \frac{da}{dt} = 0\,, \\ \frac{de}{dt} = \frac{15Gm'}{8}\frac{\sqrt{1-e^2}e}{na'^3}\sin^2 i \sin 2\omega\,, \\ \frac{di}{dt} = -\frac{15Gm'}{8}\frac{e^2}{na'^3}\sin i\cos i\sin 2\omega\,, \\ \frac{d\Omega}{dt} == -\frac{3}{8}\frac{Gm'}{na'^3\sqrt{1-e^2}}[\cos i(2+3e^2) - 5e^2\cos i\cos 2\omega]\,, \\ \frac{d\omega}{dt} = -\frac{3}{8}\frac{Gm'\sqrt{1-e^2}}{na'^3}[(1-e^2)(1-5\cos 2\omega) - 5(1-\cos 2\omega)\cos^2 i]\,. \end{cases} \tag{19}$$

We note that the system of external quadrupole moment approximation is a relatively mature field of study (Lidov 1962; Kozai 1962; Yokoyama et al. 2003; Kozai 2004; Naoz et al. 2011; Clifford 2017; Wang et al. 2018). Because there is no mean anomaly M or longitude of ascending node Ω, the canonical conjugate variables L and $H = L\sqrt{1-e^2}\cos i$ are constant, and the ratio $C = H/L$ is constant. For a given C, e increases as i decreases and vice versa. The system has a resonance about the argument of the pericenter, if $d\omega/dt = 0$, which is also known as LK-resonance (Lidov 1962; Kozai 1962). The condition is satisfied at $\omega = \pm 90°$ and $\cos i = \sqrt{3/5(1-e^2)}$. Thus, the equilibrium point is situated at $\omega = \pm 90°$, $e = [1-\sqrt{5/3}C]^{1/2}$ and $i = \arccos(\sqrt{3/5}C)^{1/2}$. This stationary solution exists if the initial condition $\sqrt{(1-e^2)}\cos i < \sqrt{5/3}$ is satisfied, and accordingly, the critical inclination, above which the LK-resonance exists, is given by $i_{\rm crit} > 39.2°$ and the amplitude of eccentricity and inclination is determined by C. The orbit of the initially high eccentricity will excite the high inclination, and for the orbit of the initially high inclination, it will excite the high eccentricity. This property is also used to explain the formation and migration mechanism of hot Jupiter exoplanets.

Since Equation (11) and Equation (19) are expressed in a uniform form – the orbital element form – we can combine the two sets of equations. When the tidal perturbation and third body perturbation are taken into account, what is the new evolution mechanism of the system? Will the system no longer generate resonance even if the inclination meets the condition of LK angular resonance? In this paper, we will try to find answers. After perturbation of the third body is considered, the orbital angular momentum of the third body should also be taken into account in angular momentum conservation. In the calculation process, the angular momentum of the system is basically constant at the previous moment and the later moment, so the above rotation equations are still applicable to the CPM.

2.5 Timescale

There are several timescales in the special tidal model, for instance, the evolution timescale of the orbital elements and those of the rotational rate and direction. Because the equations of tidal perturbation contain high terms of eccentricity, we should expand Equations (11)−(14) about e at $e = 0$ by using Taylor series, and then we can deduce the four timescales which characterize the tidal evolution of an isolated binary system. These are: i) the synchronization time $t_{\rm sync}$ is defined as

$$\begin{aligned} \frac{1}{t_{\rm sync}} &= \frac{1}{n-\Omega_p}\frac{d\Omega_p}{dt} = 3K_T \\ &= \frac{3}{I_p}[\frac{3}{2}\frac{k_2}{T_t}\frac{M^2}{m}\frac{R^8}{a^6}]\,, \end{aligned} \tag{20}$$

where the nonlinear terms of the eccentricity have been neglected and $\vartheta = 0$; ii) the circularization time $t_{\rm circ}$ is defined as

$$\frac{1}{t_{\rm circ}} = -\frac{1}{e}\frac{de}{dt} = \frac{21}{2}\frac{k_2}{T_t}\frac{QM}{m}(\frac{R}{a})^8\,, \tag{21}$$

assuming that co-rotation has already been achieved ($\Omega_p = n$; $\vartheta = 0$); iii) the equations of motion for orbital inclination and longitude of the ascending node have similar forms, and their evolutionary timescale t_i is given by

$$\frac{1}{t_i} = \frac{3}{2}\frac{k_2}{T_t}\frac{QM}{m}\Big(\frac{R}{a}\Big)^8\frac{\Omega_p}{n}\,; \tag{22}$$

iv) the equations of motion for inclination and longitude of the ascending node of the planetary equatorial plane have similar forms, and their evolutionary timescale t_I is expressed by

$$\begin{aligned}\frac{1}{t_I} &= K_T(1-e^2)^{-\frac{9}{2}} \\ &= \frac{3}{2}\frac{k_2}{I_pT_p}\frac{M^2}{m}\frac{R^8}{a^6}(1-e^2)^{-\frac{9}{2}}\,.\end{aligned} \tag{23}$$

From those timescales, we can get $t_i/t_I = \frac{M[a(1-e^2)]^{1/2}}{\sqrt{m+M}R^2r_g^2\Omega_p}$. We expect that $t_i/t_I \gg 1$, since the SMA a is much larger than the radius R of the planet and the mass M of the central object is much larger than the mass m of the planet. This is why the angle I changes quickly and then tends to the inclination i in Figure 2. Notably, while the inner SMA is larger or the eccentricity is smaller, the timescale t_I will be longer, and it will take more time for the angle ϑ to tend to zero. Accordingly, the timescale of oscillations for eccentricity and inclination of LK-resonance $t_{\rm lk}$ is given by Holman et al. (1997) and Antognini (2015)

$$t_{\rm lk} \cong \frac{32\pi Ma'}{15(G(M+m))^{1/2}m'a^{3/2}}(1-e'^2)^{3/2}\,. \tag{24}$$

Because the perturbing body is in a circular orbit, $e' = 0$ and the timescale $t_{\rm lk}$ is mainly determined by the masses of the central body, the planet, the perturbing body, and the inner and outer SMA. Equation (23) shows that the larger the initial inner SMA and the smaller the eccentricity, the larger the value of timescale t_I. Meanwhile Equation (24) implies that the larger the initial inner SMA, the smaller the value of timescale $t_{\rm lk}$.

3 THE EFFECT OF THIRD BODY PERTURBATION ON TIDAL DISSIPATION

In this and the below section, the coupling effects of tidal dissipation and third body perturbation are investigated, and the coupling results of changing the initial orbital elements are analyzed. This section will describe studies on the coupling effects of the third body perturbation and tidal dissipation, with more attention on the effect of the third body perturbation to the tidal mechanism. Anderson et al. (2016) focused on the effects of a planet's tide on a star, and the star's rotation and flattening caused by stellar rotation when the ratio of the initial SMA of the inner and outer orbits is between 0.015 and 0.035. Naoz et al. (2012) selected the initial ratio of the SMA between 0.005 and 0.05, and considered the third body perturbation as an elliptic external octagonal moment approximation (i.e., the eccentric LK mechanism, EKL). By changing the constant phase Q of tidal dissipation and using the Monte Carlo method for the associated statistics, they found that the EKL mechanism contributed 30% to the observations relative to all the hot Jupiters. In this paper, we take into account more effects, such as the rotation of the planet, the star's tidal effect on the planet and the effect of the third body, and the SMA ratio of the initial inner and outer orbits being between 0.005 and 0.1.

For conciseness, the third body mass and orbital parameters selected in this section are suitable for the following numerical calculation, unless specified otherwise. The third body mass $M' = 10^{-1}M_\odot$, orbital SMA $a' =$ 20 AU, eccentricity is zero and the orbital inclination, longitude of the ascending node and argument of pericenter are provided in Section 2.4. Since the system evolution under CPM is still related to many other parameters, the differences in system evolution could be analyzed separately by changing the initial values of the SMA, eccentricity and orbital inclination. Firstly, we compare the timescales t_I and $t_{\rm lk}$, since Equation (23) and Equation (24) are given in Section 2.5 and the relevant parameters are given in the previous parts. To improve the efficiency of the tidal mechanism, the eccentricity is assumed to be 0.8 and the rotation period is set to be 1 h in Figure 3. When the SMA increases, the timescale t_I will increase and the timescale $t_{\rm lk}$ will decrease, and vice versa. Furthermore, while the SMA a is about 0.25 AU, t_I is equal to $t_{\rm lk}$. We have performed a number of calculations. When the initial timescale t_I is less than $t_{\rm lk}$, the system will quickly enter the stable state. To reveal the coupling effect of the CMP, we chose three groups of SMA from them as the initial values in Figure 4, namely 0.3 AU, 0.5 AU and 1 AU.

Results of numerical calculations from changing the half-length diameter of orbit are shown in Figure 4. In particular, the initial orbital parameters are set to $e = 0.8$, $i = I = 60^\circ$, $\Omega = \Theta = 40^\circ$, $\omega = 5^\circ$ and $T_p = 1$ h. From the analysis in Section 2.2, we know that when the rotational direction of the planet is parallel to the normal direction of the orbital plane, then $di/dt = dI/dt = 0$ and $d\Omega/dt = d\Theta/dt = 0$. In other words, in an isolated binary system, the above equations will not change, and the orientation of rotation is consistent with the normal direction of the orbital plane. Investigating how the system would evolve as the third body perturbs to change the orbital inclination, we set $i = I$ and $\Omega = \Theta$ initially.

In Figure 4(a), initially, $a = 0.3$ AU, and the timescale t_I is 1.1×10^6 and $t_{\rm lk}$ is 3.2×10^5, which are the same order of magnitude. In detail, t_I is slightly larger than $t_{\rm lk}$.

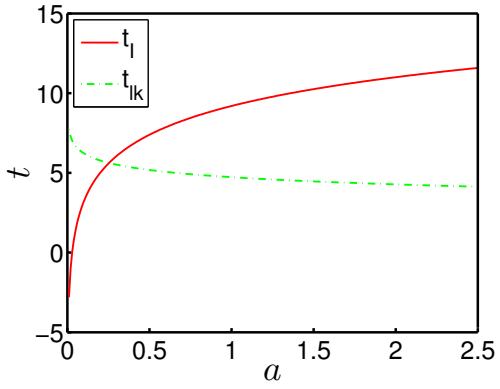

Fig. 3 Comparisons between t_I and $t_{\rm lk}$ with the change in SMA.

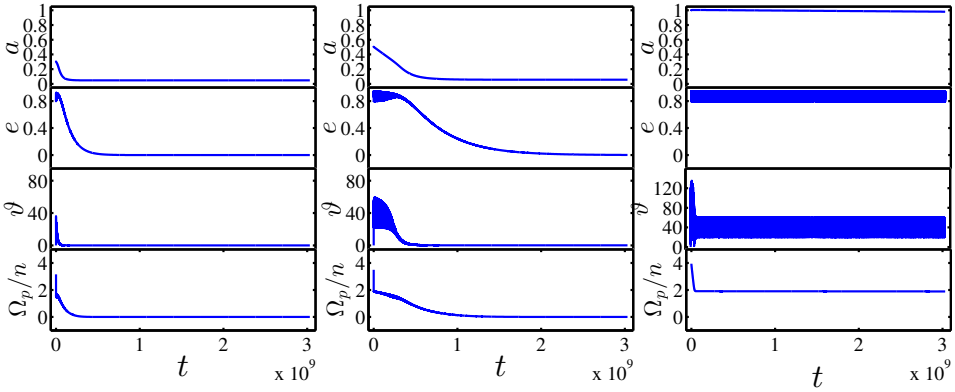

Fig. 4 System evolutions from different initial orbital SMAs under the CPM. From left to right: a, b, c.

As the SMA decays, $t_{\rm lk}$ becomes larger and t_I becomes smaller and, as a result, the included angle ϑ quickly increases from 0 to nearly 40°, and then gradually decays to a steady state. Meanwhile, the eccentricity oscillates initially and then decreases to zero. In Figure 4(b), initially, $a = 0.5\,$AU, and the timescale t_I is 2.4×10^7 and $t_{\rm lk}$ is 1.5×10^5, in which the former is about 10^2 times the latter, which means that the third body perturbation is dominant. Firstly, the eccentricity oscillates, meanwhile the included angle ϑ rises quickly to more than 60° from initial value 0, but as the SMA decreases continuously, then $t_{\rm lk}$ becomes bigger and t_I becomes smaller. As a result, the included angle ϑ declines and oscillates until back to nearly zero, and the eccentricity decays continuously to zero. Furthermore, the initial value of the SMA is enlarged continually as $a = 1.0\,$AU (see Fig. 4(c)), and the timescale t_I is 1.6×10^9 and $t_{\rm lk}$ is 5.4×10^4, in which the former is about 10^5 times the latter. Results in Figure 4(c) show that over nearly the whole evolution, the SMA seemingly does not decay, and the eccentricity is still oscillating. Due to the obvious differences in the timescales t_I and $t_{\rm lk}$, the included angle ϑ rises quickly to more than 90° from initial value 0, and the angle then quickly recedes and finally oscillates between 20° and 60°. The ratio of rotation rate and mean motion rate in Figure 4(c) also experiences a process of rapid decay, and then slowly decays.

Figure 4 demonstrates that the smaller the initial value of SMA, the smaller the timescale t_I and the greater the timescale $t_{\rm lk}$, and then the system will more quickly enter the stable state (circular, co-rotation and co-planar), which means that the normal direction of the orbital plane and the direction of rotation would rapidly enter into a consistent state. In contrast, when the SMA increases, the tidal force weakens, the third body perturbation is strong, and it will take a relatively long time to reach the same consistent state for the normal direction of the orbital plane and the orientation of rotation. While the SMA exceeds a certain range, the timescale t_I is much greater than $t_{\rm lk}$, and the third body perturbation is dominant; then the orbital inclination and eccentricity are still in an oscillating state, but the SMA has only weak attenuation. Moreover, there is a significant inconsistency between the normal direction of the orbital plane and the rotation direction, namely $\vartheta \neq 0$. Also, ϑ is oscillating and not zero, which suggests that there are mutual constraints between the direction of rotation and the normal direction of the orbital plane under the CPM, indicating that the third body perturbation has an influence on tidal dissipation.

From the above section, we know that in an isolated binary system, the rate of change of the rotational direction, orbital inclination and longitude of ascending node will quickly go to zero in the general tidal model, and then the rotational direction is parallel to the normal direction of the orbital plane with a very short timescale. Only under third body perturbation can the orbital inclination change periodically. In the CPM, the third body perturbation mechanism exciting the orbital inclination, and tidal dissipation mechanism making θ zero, have different phase and amplitude, which causes the included angle to oscillate continuously.

In Figure 5, the coupling effect is analyzed by changing the initial eccentricity. The initial orbital parameters are $a = 0.1\,\mathrm{AU}$, $i = I = 70$, $\Omega = \Theta = 10^\circ$, $\omega = 90^\circ$ and $T_p = 1\,\mathrm{h}$. Since $a = 0.1\,\mathrm{AU}$, no matter what value the eccentricity is, the timescale t_I is smaller than t_{lk}. In Figure 5(a), the initial value of eccentricity is $e = 0.8$, and the timescale t_I is 1.6×10^3 and t_{lk} is 1.7×10^6, in which the former is about 10^{-3} times the later, which means that the tidal effect is dominating. Then the attenuation of the orbital elements is dramatic, until a decays to near stability and the eccentricity rapidly decays to the circular state finally. The included angle ϑ instantaneously increases and then returns to zero again. In Figure 5(b) the initial eccentricity is $e = 0.5$ and the timescale t_I is a quarter of t_{lk}. However, attenuation of the SMA is gentle, and the eccentricity oscillates and decays gradually; as time goes on, it only decreases to about 0.3 finally. Meanwhile, the included angle ϑ rapidly grows more than 2° and damps slowly. Figure 5(c) corresponds to the case of the initial eccentricity $e = 0.1$ and the timescale t_I is approximatily equal to t_{lk}. Since the initial eccentricity is small, the tidal effect at periapsis is relatively weak, which would not appear the moment that the timescale t_I is smaller than t_{lk} in the beginning. Due to the timescale t_I being equal to t_{lk}, the third body will not excite a more eccentric orbit. As a result, the rotational direction and normal direction of the orbital plane will remain inconsistent for a longer time. When the initial eccentricity is high, the same as the tidal force, the system would enter a stable state quickly. By comparing the three sub-figures in Figure 5, some findings could be presented: (1) when $e = 0.8$, the system reaches stability after $10^8[T]$; (2) when $e = 0.1$ and $e = 0.5$, the tidal force weakens relatively at the periapsis and the third body perturbation also weakens, but $\vartheta \neq 0$ for a longer time, which also demonstrates the complicated coupling effect of the two mechanisms in the system.

Figure 6 depicts the results of changing the initial orbital inclination. The initial orbital parameters are: $a = 0.5\,\mathrm{AU}$, $e = 0.8$, $i = I$, $\Omega = \Theta = 40^\circ$, $\omega = 5^\circ$ and $T_p = 1\,\mathrm{h}$, and t_I is about 10^3 times t_{lk}. In Figure 6(a), the initial inclination is $i = 70^\circ$, and the SMA a quickly decays to a steady state; the eccentricity e firstly rises for a very short time, and then damps to the final stable case; the included angle ϑ quickly rises to nearly 70° at the beginning and rapidly reduces to zero. In Figure 6(b), the initial inclination is $i = 60^\circ$, and the angle ϑ quickly rises to nearly 60°, then oscillates and decays to 0°. In Figure 6(c), the initial inclination is $i = 30^\circ$, which is smaller than the previous two. On the scale of a billion years, a only decays weakly, and the orbital eccentricity remains oscillating; the angle ϑ fleetingly rises to more than 80°, and then quickly falls back to and oscillates around 20°. The results of Figure 6(c) illustrate that while the system has a low initial orbital inclination, the rotational direction and the normal direction of the orbital plane quickly become inconsistent from the initial consistent state, and an angle of about 20° between the two directions would exist continually in the end. In fact, when third body perturbation is taken into account, although the initial orientation of rotation and normal orientation of the orbital plane are artificially set to be consistent, there will still be inconsistency in the evolution process.

Figure 6 demonstrates that where the other parameters are the same, the smaller the initial orbital inclination, the longer the rotation direction is inconsistent with the normal direction of the orbital plane, in other words, the longer $\vartheta \neq 0$ lasts, which is the "bifurcation" phenomenon. In addition, the ratio of the rotational rate and the mean motion rate experiences a rapid decline at the beginning of evolution, regardless of whether or not it eventually evolves into a stable state or not.

In the above research, in order to simplify the variables and investigate the coupling effect of third body perturbation and tidal dissipation, the mass and SMA of the third body are set to be invariant and fixed. In fact, the influence of the mass and SMA of the third body on the system evolution can be analyzed from the expression timescale t_{lk}, Equation (24). The effect on t_{lk} when the SMA a' is reduced by one tenth is equivalent to the effect on t_{lk} when the mass of the third body is increased by one thousand times. When the mass of the third body increases or the SMA a' decreases, the effect on t_{lk} is similar to that of the increased SMA a, and then the t_{lk} will become smaller, and vice versa. If the t_{lk} is smaller than t_I, the angle ϑ will keep oscillating for a longer time. The initial orientation of rotation is set to be consistent with the initial value of the normal direction of the orbital plane, and $\vartheta = 0$. Then what if $\vartheta \neq 0$? Firstly a set of initial orbital parameters is selected: $a = 0.3\,\mathrm{AU}$, $e = 0.8$, $i = 60^\circ$, $\Omega = \Theta = 30^\circ$, $\omega = 5^\circ$ and $T_p = 1\,\mathrm{h}$, and the angle θ is changed by altering the rotational direction tilt I. The tilt I is separately set as $I = 5^\circ$, 10°, 30°, 60°, 70° and 85°, so there would be different cases: (1) $I = 60^\circ$, $\vartheta = 0$; (2) $I \leq 60^\circ$, the smaller the value of I, the greater the angle ϑ; (3) $I \geq 60^\circ$,

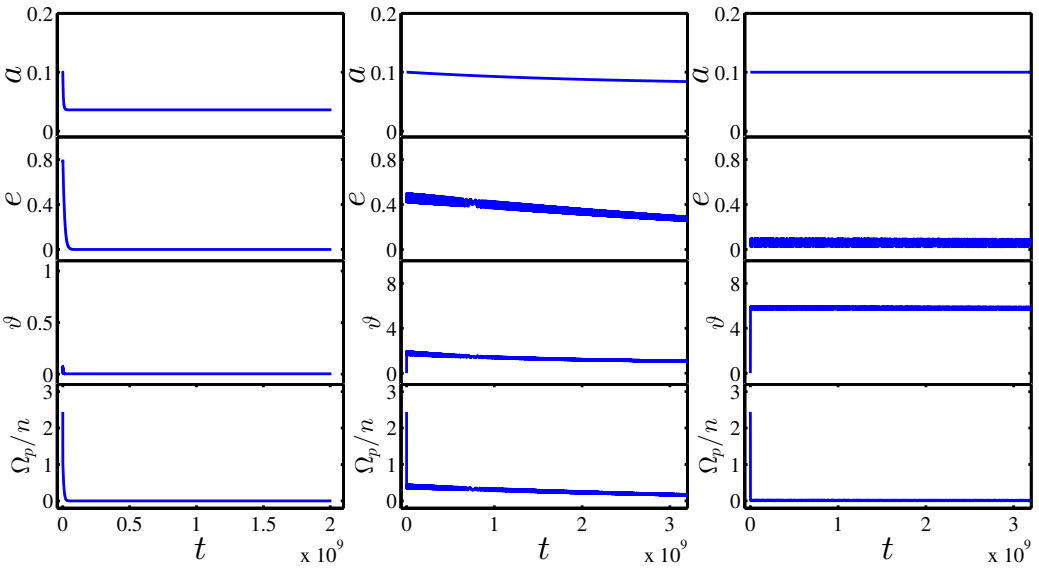

Fig. 5 System evolutions of different initial orbital eccentricities under the CPM. From left to right: a, b, c.

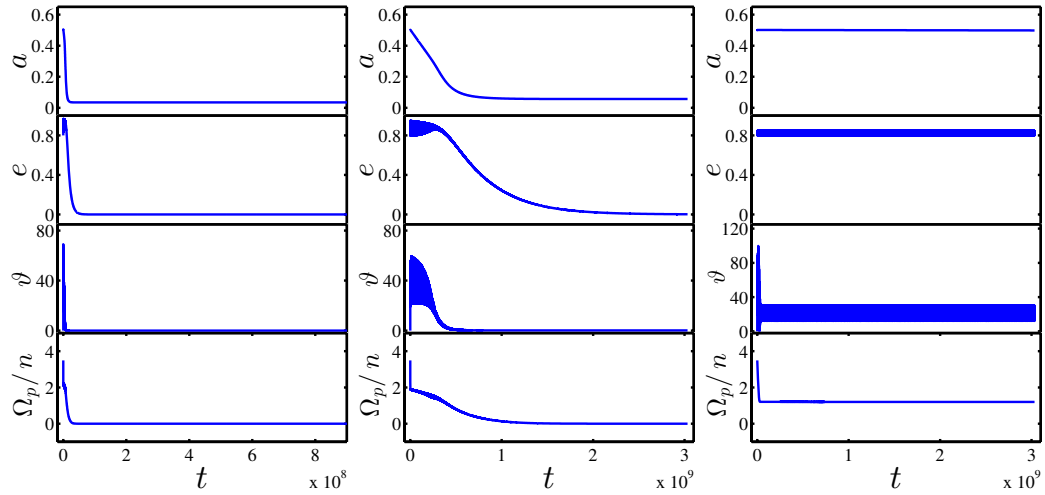

Fig. 6 System evolutions of different initial orbital inclinations under the CPM. From left to right: a, b, c.

the greater the value of I, the greater the angle θ. Among the six groups of data, the angle ϑ is largest in the case where $I = 5^\circ$. However, it can be seen from Figure 7 that, despite the initial value of $\vartheta \neq 0$, the angle ϑ rapidly goes to zero during evolution. In addition, the orbital inclinations of different initial values are stable around the same value, which means that whether the initial rotational orientation is consistent with the normal orientation of orbital plane has little influence on system evolution.

In general, the system enters a stable state of circularized coplanar corotation in billions of years, when the initial orbit has a smaller SMA, a larger eccentricity or a larger initial orbital inclination. In the process of entering a stable state, the rotational orientation and normal direction of the orbital plane firstly tend to be consistent, prior to the other parameters, and then the amplitude of ϑ gradually decreases until stable. When the initial SMA is greater, the initial eccentricity is smaller, and the initial orbital inclination is smaller. The inconsistency between rotational orientation and normal orientation of the orbital plane will continue for a longer time, and it is no longer like the case where the isolated binary system is only affected by tidal perturbation. The excitation effect of the third body perturbation on the orbital inclination and eccentricity makes the system in the CPM more likely to show a longer duration of $\vartheta \neq 0$ ('bifurcation'). From Equations (12) and (21), it can be seen that when the SMA decreases and the eccentricity becomes bigger, the tidal effect increases, meanwhile, the influence of third body perturbation becomes weaker, and vice versa. In the case where the tide is ab-

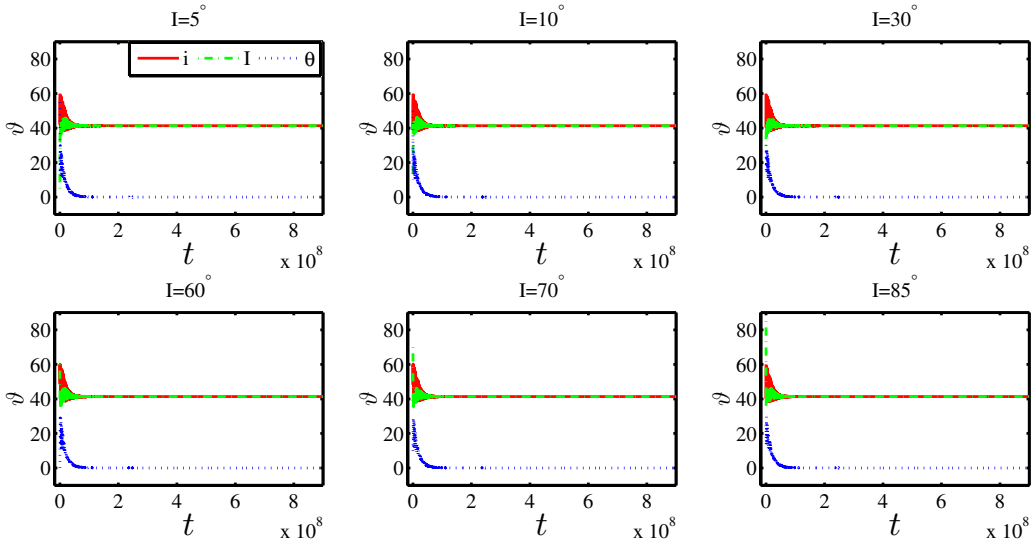

Fig. 7 Evolutions of included angle for different initial included angles.

solutely dominant, which means that the timescale t_I is much smaller than $t_{\rm lk}$, the system will evolve into a stable state; and when the third body is absolutely dominant, which means that the timescale t_I is much greater than $t_{\rm lk}$, there will be 'bifurcation' between the rotational orientation and the normal direction of the orbital plane during the evolution process, which will last for a long time and even accompany the whole evolution process. When the timescale t_I is about the same as $t_{\rm lk}$, the evolutionary path depends on whether the eccentricity is great or small. If the eccentricity is greater, then the tide will become stronger than that of the small eccentricity at periapsis, and as a result, the orbital radius will decay, which causes t_I to be smaller and $t_{\rm lk}$ to be greater. Then, the angle ϑ will tend to zero.

4 THE EFFECT OF THIRD BODY PERTURBATION ON TIDAL DISSIPATION

When the systems are eventually in a stable state, the included angle between the normal direction of the orbital plane and the rotational direction is no longer changed, namely ϑ remains zero, but the orbital plane of the planet is not consistent with the reference plane – the third body orbital plane. For a more intuitive observation of the evolution, the angle ϑ is replaced by the tilt $I(i)$ in the pictures below. Furthermore, the systems that eventually enter a stable state are selected. Specifically, three sets of initial parameters are selected, as shown in Table 1. Here, the first row of data displays the initial parameters of Figure 8(a), the second row of data features the initial parameter of Figure 8(b) and the third row of data lists the initial parameters of Figure 8(c).

Table 1 The Initial Orbital Elements and Parameters of Rotation

a(AU)	e	$i(^\circ)$	$\Omega(^\circ)$	$\omega(^\circ)$	T_p(h)	$I(^\circ)$	$\Theta(^\circ)$
0.5	0.8	60	25	5	1	60	25
2	0.01	85	25	90	1	85	25
1	0.6	85	25	90	1	85	25

In Figure 8(a), due to the effects of the third body perturbation, the eccentricity oscillates firstly with the decaying SMA caused by tidal dissipation. Meanwhile, the timescale t_I is much greater than $t_{\rm lk}$, the tilt I and the orbital inclination i have different amplitude and phase, and the tilt I instantaneously falls from 60° to about 0°. When the SMA becomes sufficiently small, which means that the tide is dominant, the tilt I and orbital inclination i enter a state of phase and amplitude consistency after a stage of inconsistency, and the eccentricity has not completely decayed to zero at this time. Thus the SMA continually decreases and the eccentricity rapidly enters the circular state after the initial oscillation attenuation. While the angles I and i are in a state of amplitude stability, the orbital inclination is 27.0°, which is below the minimum inclination of 39.2° required for LK resonance. In Figure 8(b), the initial value is in the LK resonance region, and the tidal dissipation effect is also weak. At first, the eccentricity oscillates with a receding amplitude, meanwhile, the SMA slowly recedes, which causes the timescale t_I to be smaller than the initial moment and the timescale $t_{\rm lk}$ to be larger than the initial moment. As a result, the tilt I quickly approaches the orbit inclination and then the attenuation speed of the SMA and eccentricity become more apparent until the system reaches a stable state, and finally enters the quasi-synchronous state. After synchronous attenuation, they have a stable orbital inclination of $i = 44.4^\circ$,

which is only slightly larger than the minimum vibration inclination of LK. Therefore, the orbital inclination and eccentricity would oscillate periodically with a small amplitude, when only the third body perturbation action is taken into consideration for the stable state. However, when the system is stable in the CPM, although the inclination is satisfied, the precessional motion of the argument of periapsis does not appear.

In Figure 8(c), compared with Figure 8(b), the tidal force is stronger due to the decrease of SMA, and meanwhile the effect of the third body perturbation becomes weaker. Therefore, it takes a shorter time for the rotational direction and normal direction of the orbital plane to be consistent in phase and amplitude. In the beginning, the tilt I falls quickly to around 30°, and then quickly approaches the orbital inclination, while the inclination is damping and oscillating, until they become quasi-consistent. As the third body has just made the inclination have a tiny change, the tide immediately makes the included angle ϑ become zero, and as a result, the amplitude of the tilt I and inclination i continue to attenuate until the final stable state. In other words, neither the tilt I nor the inclination i will change and ϑ stays zero. Finally, $i = 63.1^\circ$, which is obviously greater than the minimum inclination of LK resonance. Therefore, when only the third body perturbation is taken into account, the orbital inclination and eccentricity would oscillate periodically with large amplitude. However, when the system is stable in the CPM, although the inclination is satisfied, the precessional motion of the argument of periapsis does not appear. For a short summary, compared with a quickly consistent case in an isolated binary system, the rotational direction and normal direction of the orbital plane have to experience a long or short time of inconsistent amplitude and phase before a quasi-consistent state, because of the existence of the third body perturbation in the CPM. Then the two directions will undergo a process of gradual attenuation of amplitude, and finally stabilize at a certain angle. While the last stable orbital inclination has a considerable deviation from the initial value, the planetary orbital plane does not coincide with the reference plane. In addition, the ratio of the rotation rate and the mean motion rapidly decays in the initial evolution stage, then undergoes a relatively gradual decay, and finally enters into the corotation state. In Figure 8(b) and (c), the stable inclinations are greater than 39.2°, which is the minimum value for LK resonance. However, the precessional motion of the argument of periapsis does not appear, although the inclination is greater than the critical inclination. When only the third body perturbation effect is taken into account, the orbital eccentricity and inclination should show periodic oscillation, but they do not appear and the motion of the argument of periapsis is featureless and not in precession in the CPM. Results indicate that the tidal dissipation will inhibit the LK effect of the third body perturbation in the CPM, so that the system may have long-term resonance under the third body perturbation, but no longer have long-term resonance in the CPM, and the orbital inclination will be stable around a certain value.

Furthermore, the next part will investigate the distribution of orbital inclination after stabilization by changing the initial orbital elements. Firstly, the initial SMA and other initial parameters are selected: $a = 0.1$, 0.3, 0.5, 1, 1.5, $2\,\mathrm{AU}$, $e = 0.8$, $i = I = 80'$, $\Omega = \Theta = 25\Omega = \Theta$, $\omega = 5'$ and $T_p = 1\,\mathrm{h}$. As the initial SMA increases, the effect of third body perturbation becomes more important, t_I becomes greater than t_{lk}, and then the inclination will experience oscillation for a longer time. Results are shown in Figure 9; when $a = 0.1\,\mathrm{AU}$, the stable inclination is about $80'$; when $a = 0.3\,\mathrm{AU}$, the stable inclination is about $75'$. The inclination of the stable orbit decreases gradually as the value of the initial SMA increases; for $a = 2\,\mathrm{AU}$, the stable inclination is slightly greater than $35'$. In addition, in those configurations which finally enter into a stable state, the included angle ϑ may be even greater than $90'$ during the evolution (see the case where $a \geq 1\,\mathrm{AU}$ in Fig. 9).

At the top of Figure 10 the following initial orbit configuration is adopted: $a = 0.5\,\mathrm{AU}$, $e = 0.8$, $i = I$, $\Omega = \Theta = 25'$, $\omega = 5'$ and $T_p = 1\,\mathrm{h}$, and the initial orbital inclination I is set as $60'$, $70'$ and $80'$ respectively. The results at the top of Figure 10 demonstrate that the higher the initial orbital inclination, the higher the stable orbital inclination; and the larger the initial inclination, the shorter the time taken to achieve stability.

At the bottom of Figure 10, the following initial orbit configuration is adopted: $a = 0.5\,\mathrm{AU}$, $i = I = 70'$, $\Omega = \Theta = 35'$, $\omega = 5'$ and $T_p = 1\,\mathrm{h}$, and the initial eccentricity e is taken as 0.6, 0.7 and 0.8, from left to right respectively. The distribution of stable orbital inclinations indicates that the larger the eccentricity, the smaller the orbital inclination after stabilization; and as the eccentricity increases, the smaller the timescale t_I, and the shorter the time it takes for the angle ϑ to reduce to zero. Note that the constraint between the eccentricity and inclination is $C = \sqrt{1-e^2}\cos i$ in the LK effect, which is constant for a given system. For different systems, higher eccentricity and higher orbital inclination will make the initial C smaller. From this perspective the smaller the initial eccentricity and orbital inclination are, the greater the initial C and the longer time it takes for the system to enter the stable state. Furthermore, in Figure 11, the following initial orbital configuration is selected: $a = 1.5\,\mathrm{AU}$, $e = 0.2$, $i = I = 85'$, $\Omega = \Theta = 25'$, and $T_p = 1\,\mathrm{h}$, and the argument of pericenter is taken as $5'$, $30'$, $40'$, $50'$, $70'$ and $90'$ in the different panels respectively. With the increase of the argument of pericenter, the closer the system is to the LK resonance region, the more obvious the third body

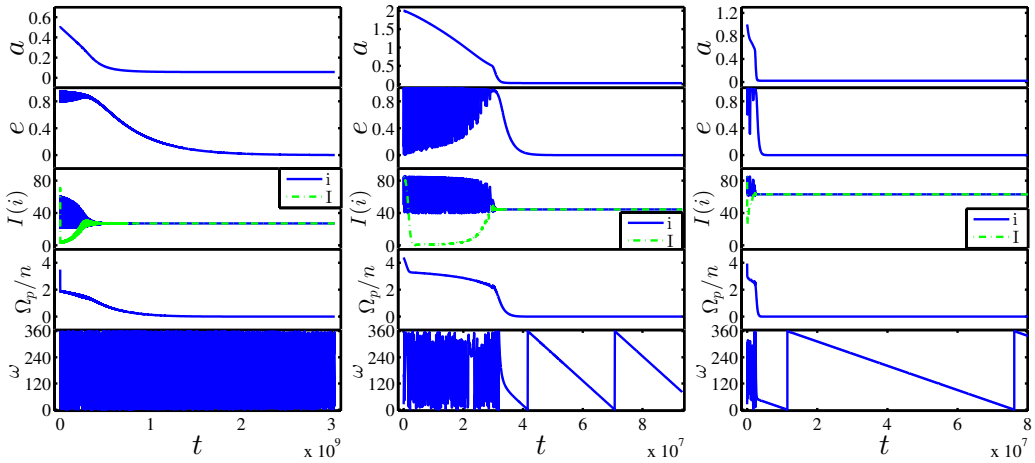

Fig. 8 The inhibitory effects of tidal dissipation on the secular effect of the third body perturbation. From left to right: a, b, c.

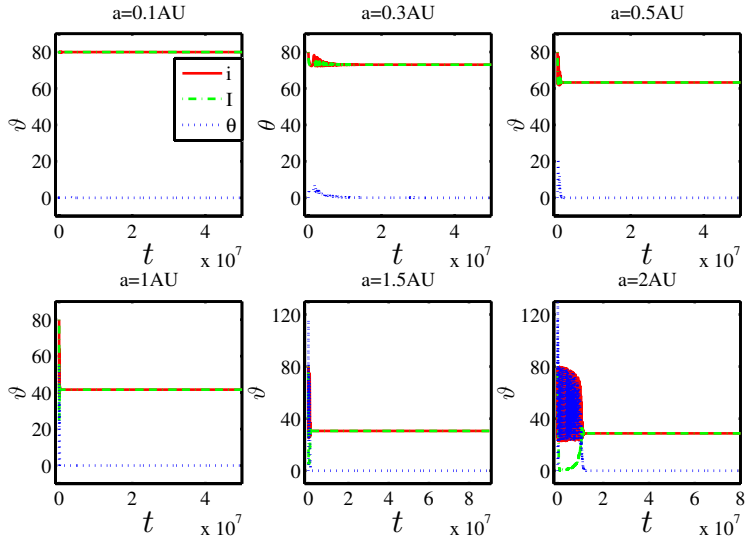

Fig. 9 Evolutions of angles under different initial SMAs.

perturbation effect is. Although the other initial values are the same, it takes longer for the system to reach a stable state as the argument of pericenter increases. In addition, the argument of pericenter in Figure 11 can be roughly divided into two categories, one is close to the equilibrium point $\pm 90'$, and the other is far from the equilibrium point $\pm 90'$, and the orbital inclination of the former is obviously greater than that of the latter after stabilization, while the orbital inclinations are not very different from each other. In general, for those stable systems, the larger the initial SMA is, the larger the eccentricity and the orbital inclination, then the larger the orbital inclination after stabilization. The influence of the initial argument of pericenter on the orbital inclination of the final stability is different: if the initial argument of pericenter is in the region close to the equilibrium point, the stabilized orbital inclination is significantly larger than that in another case, where the initial argument of pericenter is far away from the equilibrium point region.

5 CONCLUSIONS AND DISCUSSION

Tidal dissipation is the process of energy attenuation and system transformation. By tidal friction, the mechanical energy of the system is transformed into thermal energy, which gradually circulates the orbit to a stable or collision state. To reveal the evolution of a system before the stable state, this work extends the Hut model (Hut 1981) to a more general spatial case in corresponding coordinates, which could be applied to any eccentricity, inclination or included angle ϑ. Then the motion equations of orbit and rotation could be obtained under the constraint of conservation of angular momentum. Moreover, the general spatial tidal model provides a model framework for analyzing the ϑ and specific calculation formula. When the ro-

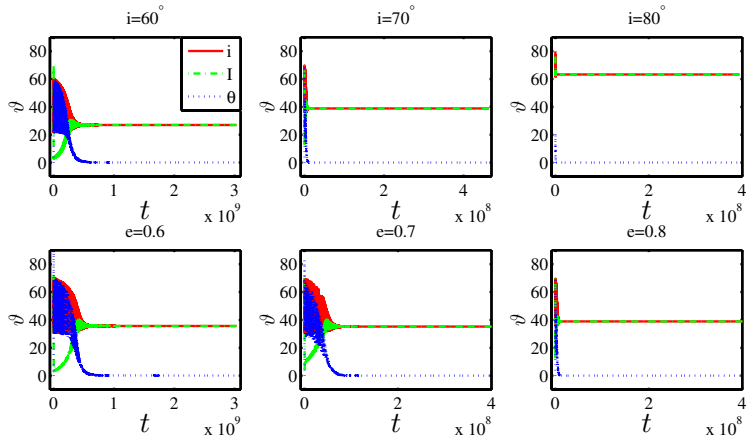

Fig. 10 Evolutions of angles under different initial inclinations and eccentricities.

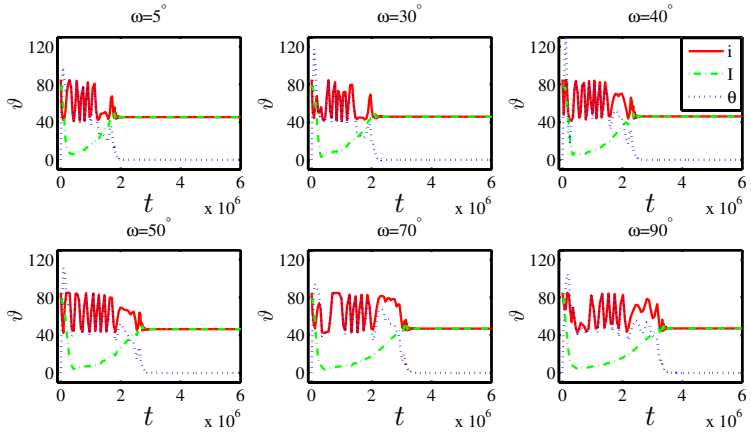

Fig. 11 Evolutions of angles under different initial arguments of periapsis.

tational orientation is consistent with the normal orientation of the orbital plane, the general spatial model will degrade to the Hut model. In an isolated binary system, the above two directions will tend to consistency rapidly with a shorter timescale t_I relative to the whole evolution process, as shown in Figure 2.

In fact, another effect such as the third body perturbation would make the eccentricity and inclination oscillate significantly with a timescale $t_{\rm lk}$, and then make the rotational direction and normal direction of the orbital plane inconsistent instantaneously, and even lead to significant qualitative change in the system if only tidal dissipation is considered. To study the coupling effect between tidal friction and third body perturbation, we adopt a circular external quadrupole approximation as the third body perturbation, and then obtain the CPM. The difference between the timescale t_I and $t_{\rm lk}$ will influence the evolution path, in which the timescale depends on the orbital elements, namely the SMA, eccentricity and even the inclination.

Compared with the widely stratified structure (Naoz et al. 2012; Anderson et al. 2016), the initial SMA ratio of the inner and outer orbits in this paper is between 0.005 and 0.1, which is more similar to the close system. We have found that if t_I is much larger than $t_{\rm lk}$, which means the tidal mechanism plays a supporting role, the system will experience sustained oscillations of eccentricity and included angle ϑ over the whole evolution, and even the rotational direction would be perpendicular to the orbital plane of the third body in the evolution process. Meanwhile, the decay of the SMA would make t_I small, even smaller than $t_{\rm lk}$, and then the included angle ϑ would also decay. If t_I is much smaller than $t_{\rm lk}$, namely, the tidal mechanism is dominant, the oscillation time of ϑ is short, and the eccentricity will decay rapidly with a slight oscillation until it reaches zero, and the system ultimately enters the stable circular coplanar corotation state. Before entering a stable state, ϑ decays to nearly zero firstly, in other words, the rotation direction tends to be the same as the normal direction of the orbital plane. After that process, the amplitude of the tilt (I, i) decays gradually until the tilt is stable around a certain value, as shown in Figures 9−11. All the above conclusions are based on the initial included angle $\vartheta = 0$, and even if $\vartheta \neq 0$ at the initial setup, there is no sig-

nificant effect on the evolution of the system, as depicted in Figure 7.

Since the system is dissipative in the CPM, dissipation will always exist if stability or collision is not reached. Those systems with an oscillating angle ϑ are unstable generally during the evolution, and they will either reach a stable state or collide eventually. However, the long-term existence of the included angle indicates that it is necessary to consider the spatial tidal model when studying the coupling effect of the tidal dissipation and the third body. In the CPM, systems that enter into the circular coplanar corotation state can be roughly divided into two categories: (1) the stable inclination is below $39.2°$, see Figure 8(a); (2) the stable inclination is greater than $39.2°$, see Figures 8(b) and (c). The higher the initial argument of pericenter is (consider $0° \sim 90°$), the higher the initial orbital inclination, the higher the initial eccentricity, the bigger the initial SMA and then the higher the orbital inclination of the stable state. After entering the stable state, if only the third body perturbation effect is considered, for the former category, the system will remain unchanged for a long time, while the latter will have periodic resonance, and the eccentricity and tilt will oscillate periodically. The above description indicates that tidal dissipation inhibits the secular resonance of the third body perturbation. In other words, for those planets that entered the inner orbit through the LK effect in a multi-body system, if tidal dissipation is considered, high orbital inclination may be maintained after stabilization. This provides a possible mechanism for explaining orbital migration in multi-body systems.

There is a wide variety of exoplanets found at present, and a certain number are located in binary or multi-star systems with large eccentricities and higher orbital inclinations. This paper mainly focuses on the possible evolution process of a system under the comprehensive mechanism of tidal dissipation and third body perturbation, without the evolution of a specific exoplanet. Research into the coupling effect of tide and third body perturbation helps in understanding the formation of exoplanets and different orbital migration mechanisms. If the rotation of exoplanets can be detected in the future, the inconsistency found in this paper and the suppression of secular effect by tidal dissipation may also aid the understanding of those exoplanets whose direction of rotation is not perpendicular to their orbital plane and these exoplanets which have a stable high inclination with no resonance caused by the third body. There are still so many questions about determining the related parameters while applying the tidal model to exoplanet evolution. Factors such as thermal tide, inertial wave tide and rotation deformation should be taken into account. Furthermore, as for the constant-τ delay model, the time delay $\tau = 0.6$ s adopted in this paper is based on the value of tidal dissipation of gas giant planets in the solar system. τ is related to the inner composition and structure of the object, which is difficult to measure. In addition, the orbital inclination and rotation direction parameters adopted in this paper are artificially set up; these parameters are difficult to obtain when the CPM is applied to the evolution of exoplanets. Due to the limitations of observing technology, the orbital inclination of only some exoplanets can be measured at present, which is also a predicament for many studies of their associated orbital evolution.

In addition, the above research is aimed at planetary tidal deformation, and it can be generalized to stellar tidal deformation or to cases of tidal dissipation of both planet and star. The spatial tidal model can be applied to any binary system with high eccentricity and high inclination, and can be directly added to other perturbations due to the perturbation function and Lagrange motion equation. While the third body is in a circular orbit, the octupole order vanishes and the hexadecapole order plays a weak role in the external perturbation. When the hexadecapole order is considered, the conclusion is similar to that of the quadrupole, which is the reason why the quadrupole has just been considered in this paper. Further, the elliptic approximation of higher order will be considered in the CPM due to the fact that the octupole can do an orbit flip.

Acknowledgements This work was supported by the National Natural Science Foundation of China (Grant Nos. 11673053 and 11673049).

References

Aksnes, K., & Franklin, F. A. 2001, AJ, 122, 2734
Alexander, M. E. 1973, Ap&SS, 23, 459
Anderson, K. R., Storch, N. I., & Lai, D. 2016, MNRAS, 456, 3671
André, Q., Barker, A. J., & Mathis, S. 2017, A&A, 605, A117
Antognini, J. M. O. 2015, MNRAS, 452, 3610
Arras, P., & Socrates, A. 2010, ApJ, 714, 1
Auclair-Desrotour, P., Laskar, J., & Mathis, S. 2017, A&A, 603, A107
Auclair-Desrotour, P., Mathis, S., & Laskar, J. 2018a, A&A, 609, A118
Auclair-Desrotour, P., Mathis, S., Laskar, J., & Leconte, J. 2018b, A&A, 615, A23
Auclair-Desrotour, P., Mathis, S., & Le Poncin-Lafitte, C. 2015, A&A, 581, A118
Barge, P., Baglin, A., Auvergne, M., et al. 2008, A&A, 482, L17
Beust, H., Augereau, J.-C., Bonsor, A., et al. 2014, A&A, 561, A43
Bodenheimer, P., Lin, D. N. C., & Mardling, R. A. 2001, ApJ, 548, 466

Breton, S., Bolmont, E., Tobie, G., Mathis, S., & Grasset, O. 2018, in SF2A-2018: Proceedings of the Annual Meeting of the French Society of Astronomy and Astrophysics, 195
Ceillier, T., van Saders, J., García, R. A., et al. 2016, MNRAS, 456, 119
Clifford, M. W. 2017, Phys. Rev. D, 96, 023017
Darwin, G. H. 1879, Philosophical Transactions of the Royal Society of London Series I, 170, 447
Darwin, G. H. 1880, Philosophical Transactions of the Royal Society of London Series I, 171, 713
Dong, Y., & Ji, J. 2012, Science China Physics, Mechanics & Astronomy, 55, 872
Eggleton, P. P., Kiseleva, L. G., & Hut, P. 1998, ApJ, 499, 853
Faber, J. A., Rasio, F. A., & Willems, B. 2005, Icarus, 175, 248
Ferraz-Mello, S., Rodríguez, A., & Hussmann, H. 2008, Celestial Mechanics and Dynamical Astronomy, 101, 171
Gold, T., & Soter, S. 1969, Icarus, 11, 356
Goldreich, P. 1963, MNRAS, 126, 257
Goldreich, P., & Soter, S. 1966, Icarus, 5, 375
Guillot, T., Lin, D. N. C., Morel, P., Havel, M., & Parmentier, V. 2014, in EAS Publications Series, 65, EAS Publications Series, 327
Heller, R., Leconte, J., & Barnes, R. 2011, A&A, 528, A27
Henning, W. G., & Hurford, T. 2014, ApJ, 789, 30
Holman, M., Touma, J., & Tremaine, S. 1997, Nature, 386, 254
Hugh, J. R. A., Butler, R. P., Tinney, C. G., et al. 2006, MNRAS, 369, 249
Husnoo, N., Pont, F., Mazeh, T., et al. 2012, MNRAS, 422, 3151
Hut, P. 1980, A&A, 92, 167
Hut, P. 1981, A&A, 99, 126
Ibgui, L., Spiegel, D. S., & Burrows, A. 2011, ApJ, 727, 75
Jackson, B., Greenberg, R., & Barnes, R. 2008a, ApJ, 678, 1396
Jackson, B., Greenberg, R., & Barnes, R. 2008b, ApJ, 681, 1631
Kalas, P., Graham, J. R., Chiang, E., et al. 2008, Science, 322, 1345
Kaula, W. M. 1964, Reviews of Geophysics and Space Physics, 2, 661
Keivan, S. G., Oelkers, R. J., Pepper, J., et al. 2018, AJ, 156, 102
Kostov, V. B., Orosz, J. A., Welsh, W. F., et al. 2016, ApJ, 827, 86
Kozai, Y. 1962, AJ, 67, 591
Kozai, Y. 1965, PASJ, 17, 395
Kozai, Y. 2004, Proceedings of the Japan Academy, Series B, 80, 157
Lai, D. 2012, MNRAS, 423, 486
Lanza, A. F. 2010, A&A, 512, A77
Leconte, J., Chabrier, G., & Baraffe, I. 2010b, in IAU Symposium, 276, The Astrophysics of Planetary Systems: Formation, Structure, and Dynamical Evolution, eds. A. Sozzetti, M. G. Lattanzi, & A. P. Boss, 248
Leconte, J., Chabrier, G., Baraffe, I., & Levrard, B. 2010a, A&A, 516, A64
Lidov, M. L. 1962, Planet. Space Sci., 9, 719
Marcy, G., Butler, R. P., Fischer, D., et al. 2005, Progress of Theoretical Physics Supplement, 158, 24
Mardling, R. A. 2007, MNRAS, 382, 1768
Mayor, M., & Queloz, D. 1995, Nature, 378, 355
Mazeh, T. 2008, in EAS Publications Series, 29, eds. M.-J. Goupil, & J.-P. Zahn, 1
Naoz, S., Farr, W. M., Lithwick, Y., Rasio, F. A., & Teyssandier, J. 2011, Nature, 473, 187
Naoz, S., Farr, W. M., & Rasio, F. A. 2012, ApJ, 754, L36
Peale, S. J., & Cassen, P. 1978, Icarus, 36, 245
Peale, S. J., & Lee, M. H. 2002, Science, 298, 593
Pont, F. 2009, MNRAS, 396, 1789
Poppenhaeger, K., & Wolk, S. J. 2014, A&A, 565, L1
Rasio, F. A., Tout, C. A., Lubow, S. H., & Livio, M. 1996, ApJ, 470, 1187
Showman, A. P., & Malhotra, R. 1997, Icarus, 127, 93
Socrates, A., Katz, B., & Dong, S. 2012, arXiv:1209.5724
Storch, N. I., Anderson, K. R., & Lai, D. 2014, Science, 345, 1317
Storch, N. I., & Lai, D. 2014, MNRAS, 438, 1526
Tobie, G., Mocquet, A., & Sotin, C. 2005, Icarus, 177, 534
Turbet, M., Bolmont, E., Leconte, J., et al. 2018, A&A, 612, A86
Wang, W. L., Q., X., Zhou, Y. H., & Liao, X. H. 2018, Progress in Astronomy, 36, 325
Welsh, W. F., Orosz, J. A., Carter, J. A., et al. 2012, Nature, 481, 475
Wisdom, J. 2004, AJ, 128, 484
Wisdom, J. 2008, Icarus, 193, 637
Wu, Y. 2018, AJ, 155, 118
Xue, Y., Suto, Y., Taruya, A., et al. 2014, ApJ, 784, 66
Yoder, C. F., & Peale, S. J. 1981, Icarus, 47, 1
Yokoyama, T., Santos, M. T., Cardin, G., & Winter, O. C. 2003, A&A, 401, 763
Zahn, J.-P. 1977, A&A, 57, 383